Journal of Sound and Vibration 329 (2010) 3632–3646

Contents lists available at ScienceDirect

Journal of Sound and Vibration

journal homepage: www.elsevier.com/locate/jsvi

Review

Periodic shunted arrays for the control of noise radiation in an enclosure

Filippo Casadei [a,*], Lorenzo Dozio [b], Massimo Ruzzene [a], Kenneth A. Cunefare [c]

[a] The Guggenheim School of Aerospace Engineering, Georgia Institute of Technology, Atlanta, GA 30332, USA
[b] Dipartimento di Ingegneria Aerospaziale, Politecnico di Milano, via La Masa, 34-20156 Milano, Italy
[c] The Woodruff School of Mechanical Engineering, Georgia Institute of Technology, Atlanta, GA 30332, USA

ARTICLE INFO

Article history:
Received 26 January 2010
Received in revised form
31 March 2010
Accepted 7 April 2010
Handling Editor: L. Huang
Available online 24 April 2010

ABSTRACT

This work presents numerical and experimental investigations of the application of a periodic array of resistive–inductive (RL) shunted piezoelectric patches for the attenuation of broadband noise radiated by a flexible plate in an enclosed cavity. A 4×4 lay-out of piezoelectric patches is bonded to the surface of a rectangular plate fully clamped to the top face of a rectangular cavity. Each piezo-patch is shunted through a single RL circuit, and all shunting circuits are tuned at the same frequency. The response of the resulting periodic structure is characterized by frequency bandgaps where vibrations and associated noise are strongly attenuated. The location and extent of induced bandgaps are predicted by the application of Bloch theorem on a unit cell of the periodic assembly, and they are controlled by proper selection of the shunting circuit impedance. A coupled piezo-structural-acoustic finite element model is developed to evaluate the noise reduction performance. Strong attenuation of multiple panel-controlled modes is observed over broad frequency bands. The proposed concept is tested on an aluminum plate mounted in a wooden box and driven by a shaker. Experimental results are presented in terms of pressure responses recorded using a grid of microphones placed inside the acoustic box.

© 2010 Elsevier Ltd. All rights reserved.

Contents

1. Introduction . . . 3633
2. Piezo-structural-acoustic model . . . 3634
3. Frequency wavenumber comparison between *in vacuo* and fluid-loaded pates . . . 3635
4. Wave propagation in periodic plates . . . 3638
5. Numerical analysis of the performance of periodic plate . . . 3642
6. Experimental test . . . 3644
7. Conclusions . . . 3646
Acknowledgments . . . 3646
References . . . 3646

* Corresponding author.
E-mail address: filippo.casadei@gatech.edu (F. Casadei).

0022-460X/$ - see front matter © 2010 Elsevier Ltd. All rights reserved.
doi:10.1016/j.jsv.2010.04.003

1. Introduction

Over the last decades, research on effective methods for suppressing cabin interior noise and vibration level has been very active in automobile and aircraft industries [1,2]. Radiated noise in acoustic enclosures is due to the coupling between vibration of the flexible boundaries and motion of the interior fluid. Increasing customer demand and awareness for improved comfort environments have prompted researchers into studying the fundamental phenomena which govern the structural-acoustic coupling and investigating innovative techniques to reduce interior noise levels. Lightweight solutions are needed which can provide global broadband noise control inside the cabin without compromising vehicle performance and efficiency. It is known that classical passive solutions such as acoustic blankets add considerable weight and are effective only at high frequencies.

About 20 years ago, Fuller and his co-workers [3,4] started to investigate the possibility of reducing aircraft interior noise by actively controlling the fuselage vibration through mechanical actuators. This approach, denoted as active structural acoustic control, has received increasing attention in the academic community, and promising results have been reported using lightweight smart devices such as inertial and piezoelectric actuators [5–7]. However, it is generally acknowledged that there is still a gap to be covered to make this technology practical due to global performance, instability issues, complexity of the controller and cost of the system.

Piezoelectric shunt damping is an attractive technique for control of vibrating structures which offers a simpler and more cost-effective solution to actively controlled piezos. Contrary to active control strategies, the key element is a passive electrical network directly connected to the electrodes of the piezoelectric device. As such, no error sensing device is required and the stability of the coupled system is guaranteed. An elegant formulation of passive shunting was first proposed by Hagood and Von Flotow [8] and is still most commonly used. The study showed how a piezoelectric material shunted through a series RL circuit, i.e., a resonant shunt, exhibits a behavior very similar to the well known mechanical tuned vibration absorber. A resonant shunt is simple to design and it offers effective damping in the vicinity of a selected mode of the underlying structure.

After the initial introduction of single-mode resonant shunts, more complex shunting circuits have been investigated for suppressing multiple structural modes. Hollkamp [9] was able to suppress two modes of a cantilever beam using a system of RLC circuits connected in parallel. The whole circuit requires as many parallel branches as there are modes to be controlled. Since no closed-form tuning solution is available for determining the component values, the method relies on the numerical optimization of a nonlinear objective function fully parametrized by all of the circuit elements. As an alternative, Wu [10] proposed the use of parallel RL shunts, each targeting an individual mode. Current-blocking LC networks are introduced in each parallel branch to reduce cross-coupling and achieve multiple resonances at the desired frequencies. Specifically, each LC circuit is tuned to the frequency of an adjacent mode in order to decouple the branches. The complexity of the circuit topology greatly increases as the number of modes to be simultaneously damped increases. More recently, the current-flowing concept was presented by Behrens et al. [11]. Compared to current-blocking schemes, the current-flowing method is simpler to tune and involves less electrical components, however it appears less effective for densely spaced modes.

In addition to the RL-based shunting techniques described thus far, other different strategies are available for multimode vibration reduction with piezoelectric shunts. The most common method is based on negative capacitance shunting as originally proposed by Forward [12]. In this configuration, a piezoelectric patch is shunted through a passive circuit connected to a negative impedance converter, so that the internal capacitance of the piezo is artificially cancelled and the impedance of the shunt circuit reduces to that of the passive circuit. If this impedance is frequency-independent, i.e., if a resistance is used, broadband damping can be achieved. Although the negative capacitance shunting strategy has been experimentally validated with success, it must be used with caution since it requires active elements that can destabilize the structure if improperly tuned. Moreover, the circuit should be tuned very close to the stability limit to achieve best performance [13].

Application of the foregoing shunting methods is not limited to vibration-only studies. In the past few years, researchers have investigated the suitability and performance of piezoelectric shunt damping to increase the acoustic transmission loss in structures. Ahmadian and Jeric [14] and Kim and Lee [15] have compared the sound transmission loss performance of plates with sound-absorbing material and RL-shunted piezo-patches. Multimode shunt damping with blocking circuit (Wu's solution) has been applied by Kim and Kim [16] for noise reduction of a plate in an acoustic tunnel. Kim and Jung [17,18] also studied broadband reduction of noise radiated by plates with multiple resonant and negative-capacitance-converter shunt circuits, and achieved good levels of noise attenuation over a limited number of modes.

A rather different approach to broadband vibration attenuation using shunts was proposed by Thorp et al. [19,20] This concept involves a periodic array of simple RL-shunted piezos mounted on the structure to passively control the propagation of elastic waves and the subsequent vibration field. Periodically induced impedance-mismatch zones generate broad stop bands, i.e., frequency bands where waves are attenuated. The tunable characteristics of shunted piezo-patches allow the equivalent mechanical impedance of the structure to be tuned so that stop bands are generated over desired frequency ranges. The presence of a shunting resistance (R) generates a damped resonance of the electrical network that allows the energy dissipation mechanism of shunted piezos to be exploited to dampen the amplitude of vibration also outside the stop bands. The original periodic shunting concept was numerically demonstrated on rods and fluid-loaded axisymmetric shells in [19,20]. More recently, this strategy was extended to flat plates [21], where Bloch theorem was used

to predict the dispersion properties of the resulting periodic assembly. The consistency of the method and its effectiveness over a broad frequency range have been validated experimentally on a cantilever aluminum plate hosting a periodic layout of 4 $\times$ 4 RL-shunted piezo-patches [22].

The present work extends the wave propagation approach presented in [22] to achieve broadband reduction of noise radiated from a plate in an acoustic cavity. A fully coupled finite element (FE) model is developed to predict the response of the piezo-structural-acoustic system. The Bloch theorem is applied to predict the dispersion relations and the corresponding stop bands of the system, and is performed on the *in vacuo* plate-piezo-patch unit-cell, i.e., neglecting the structural-acoustic coupling. Such approximation is verified by comparing the frequency bands where the acoustic energy in the cavity is reduced with those predicted by the unit-cell results. Experimental results are finally presented to validate the concept.

The paper is organized into seven sections including this introduction. Section 2 presents the variational formulation used to derive a FE approximation of the piezo-structural-acoustic system. In Section 3 the wave propagation characteristics of *in vacuo* and fluid-loaded plates are compared and it is demonstrated that the dispersion properties of the considered structural-acoustic system can be computed, as a first approximation, by neglecting the acoustic coupling. Section 4 focuses on the description of the FE-based approach for the evaluation of the wave propagation characteristics of the 2D periodic structure. Section 5 illustrates the concept of structure-borne noise reduction with periodic shunts through numerical examples and highlights the ability of the unit-cell analysis to predict the frequency regions of noise attenuation. An experimental validation of the method is described in Section 6. Finally, Section 7 summarizes the obtained results and provides some conclusions.

2. Piezo-structural-acoustic model

This section illustrates the finite element (FE) formulation adopted for the dynamic response analysis of a piezoelectric structure coupled with an air cavity. The structure is supposed to be linearly elastic and the piezo-patches are considered perfectly bonded on one surface of the plate.

Applying classical finite element procedures, the transverse displacement $w(x,y)$ of the plate is discretized with 4-node Kirchhoff elements while the acoustic cavity is divided into cubic 8-node elements with the sound pressure as the sole degree of freedom per node [23,24]. Assuming harmonic motion, the equilibrium equations of the discretized acousto-electro-elastic system are written as

$$\left(\begin{bmatrix} \mathbf{K}_{uu} & \mathbf{K}_{u\phi} & -\mathbf{C}_{up} \\ \mathbf{K}_{u\phi}^{\mathrm{T}} & \mathbf{K}_{\phi\phi} & \mathbf{0} \\ \mathbf{0} & \mathbf{0} & \mathbf{K}_{pp} \end{bmatrix} - \omega^2 \begin{bmatrix} \mathbf{M}_{uu} & \mathbf{0} & \mathbf{0} \\ \mathbf{0} & \mathbf{0} & \mathbf{0} \\ \rho_0 \mathbf{C}_{up}^{\mathrm{T}} & \mathbf{0} & \mathbf{M}_{pp} \end{bmatrix}\right) \begin{Bmatrix} \mathbf{d}_0 \\ \phi_0 \\ \mathbf{p}_0 \end{Bmatrix} = \begin{Bmatrix} \mathbf{f}_0 \\ \mathbf{q}_0 \\ \mathbf{0} \end{Bmatrix} \tag{1}$$

where $\mathbf{d}_0$ denotes the structural degrees of freedom, $\boldsymbol{\varphi}_0$ the electric potential degrees of freedom, and $\mathbf{p}_0$ the pressure degrees of freedom. Also the sub-matrices that compose the coupled system are defines as

$$\mathbf{M}_{uu} = \int_{V_s} \mathbf{N}_u^{\mathrm{T}} \rho_s \mathbf{N}_u \, \mathrm{d}V, \quad \mathbf{K}_{uu} = \int_{V_s} \mathbf{B}_u^{\mathrm{T}} \mathbf{C} \mathbf{B}_u \, \mathrm{d}V, \quad \mathbf{K}_{u\phi} = \int_{V_s} \mathbf{B}_u^{\mathrm{T}} \mathbf{e}^{\mathrm{T}} \mathbf{B}_\phi \, \mathrm{d}V$$

$$\mathbf{M}_{pp} = \frac{1}{c_0^2} \int_{V_f} \mathbf{N}_p^{\mathrm{T}} \mathbf{N}_p \, \mathrm{d}V, \quad \mathbf{K}_{pp} = \int_{V_f} \mathbf{B}_p^{\mathrm{T}} \mathbf{B}_p \, \mathrm{d}V, \quad \mathbf{K}_{\phi\phi} = -\int_{V_s} \mathbf{B}_\phi^{\mathrm{T}} \varepsilon \mathbf{B}_\phi \, \mathrm{d}V$$

$$\mathbf{C}_{up} = \int_{\Sigma} \mathbf{N}_u^{\mathrm{T}} \mathbf{N}_p \, \mathrm{d}S, \quad \mathbf{f} = \int_{S_f} \mathbf{N}_u^{\mathrm{T}} \overline{f} \, \mathrm{d}S, \quad \mathbf{q} = -\int_{S_q} \mathbf{N}_\phi^{\mathrm{T}} \overline{q} \, \mathrm{d}S \tag{2}$$

and $\mathbf{B}_u = \mathbf{D}\mathbf{N}_u$, $\mathbf{B}_\phi = \nabla \mathbf{N}_\phi$, $\mathbf{B}_p = \nabla \mathbf{N}_p$, where $\mathbf{D}$ is the linear differential operator matrix which relates the strains to the structural displacements.

This general FE formulation is here applied to the flexural vibration of a rectangular thin plate hosting a generic number of RL-shunted piezos and coupled with a rectangular acoustic cavity that has five rigid walls. The piezoelectric patches are assumed to have through-thickness polarization with electrodes connected to the top and bottom surfaces. It is also assumed that the electric potential varies linearly through the thickness, from zero at the bottom surface to ϕ_{p0} at the top electrode. Therefore,

$$\phi_0(x,y,z) = \phi_0(z) = \frac{z - h/2}{h_p} \phi_{p0} \tag{3}$$

where h and h_p are the plate and piezo-thickness, respectively. Under these assumptions, the electrical equation becomes a scalar relation of the form

$$\mathbf{K}_{u\phi}^{\mathrm{T}} \mathbf{d}_0 + k_{\phi\phi} \phi_{p0} = q_{e0} \tag{4}$$

where $q_{e\,0}$ is the external harmonic charge at the electrodes and it is related to the potential ϕ_{p0} by the impedance of the shunting circuit $Z_{\mathrm{SH}}(\omega) = R + \mathrm{j}\omega L$:

$$\phi_{p0} = \mathrm{j}\omega Z_{\mathrm{SH}}(\omega) q_{e0} \tag{5}$$

In Eq. (5) R is the resistance and L is the inductance of the circuit. Substituting Eq. (5) into Eq. (4) and then back into Eq. (1) yields

$$\left(\begin{bmatrix} \mathbf{K}_{uu} + \mathbf{S}_{Z_{SH}}(\omega) & -\mathbf{C}_{up} \\ \mathbf{0} & \mathbf{K}_{pp} \end{bmatrix} - \omega^2 \begin{bmatrix} \mathbf{M}_{uu} & \mathbf{0} \\ \rho_0 \mathbf{C}_{up}^{\mathrm{T}} & \mathbf{M}_{pp} \end{bmatrix} \right) \begin{Bmatrix} \mathbf{d}_0 \\ \mathbf{p}_0 \end{Bmatrix} = \begin{Bmatrix} \mathbf{f}_0 \\ \mathbf{0} \end{Bmatrix} \tag{6}$$

where

$$\mathbf{S}_{Z_{SH}} = -\mathrm{j}\omega \mathbf{K}_{u\phi} \left(\mathrm{j}\omega k_{\phi\phi} - \frac{1}{Z_{SH}} \right)^{-1} \mathbf{K}_{u\phi}^{\mathrm{T}} \tag{7}$$

is the shunting matrix.

3. Frequency wavenumber comparison between *in vacuo* and fluid-loaded pates

First, an attempt is made to gain insights about the dispersion properties of the coupled plate-cavity system. The variation of natural frequencies and mode shapes for different plate-enclosure configurations is analyzed in order to estimate the influence of the acoustic coupling on the dispersion properties of the structure. The goal is to demonstrate that the wave propagation characteristics of the considered piezo-structural-acoustic system may be estimated, as a first approximation, by simply neglecting the acoustic coupling. As illustrated in Section 4, this will allow for an efficient calculation of the dispersion properties of the system based on the unit-cell analysis approach conducted on the *in vacuo* plate.

The considered host structure consists of a rectangular fully clamped aluminum plate measuring $600 \times 400 \times 1$ mm. The panel hosts a periodic array of 4×4 square piezoelectric patches perfectly bonded to one side (see Fig. 5(a)). The geometric and material properties of the plate and piezo-patch are illustrated in Tables 1 and 2. The plate can be considered as the result of a 4×4 assembly of unit cells measuring 150×100 mm. During this analysis, the piezo-shunts are maintained in the short circuit configuration, i.e., $Z_{SH} \to 0$, in order not to introduce any complexity of the electrical impedance in the dynamic stiffness matrix formulation of Eq. (6).

Numerical simulations are carried out for two different cavity configurations as illustrated in Fig. 1: first the smart plate is placed at the top of a rectangular shaped air cavity, denoted as cavity 1, of dimensions $600 \times 400 \times 500$ mm. Second, a smaller enclosure, here denoted as cavity 2, with sides $600 \times 400 \times 200$ mm, is also considered in order to verify the effectiveness and robustness of the present approach. The remaining five walls of the considered cavities are assumed to be rigid.

Comparing the natural frequencies of the uncoupled and coupled plate–cavity system, part of which are summarized in Table 3, it is possible to observe that modes "controlled" by the vibration of the plate have natural frequencies slightly lower than those of the uncoupled plate modes. Similarly, the natural frequencies of the modes "controlled" by the acoustic vibrations in the enclosure are slightly higher than those of the corresponding uncoupled cavity modes. In either case the variation of the frequencies is modest and in this specific case never exceeds 1.0 percent. The comparison between the *in vacuo* and fluid-loaded panel-controlled mode shapes is then considered in order to estimate the change of the

Table 1
Geometry and physical properties of the clamped plate.

Parameter	Value
Dimensions	$600.0 \times 400.0\,\mathrm{mm}^2$
Thickness	1.0 mm
Mass density	$2730\,\mathrm{kg/m}^3$
Young's modulus	$7.0 \times 10^{10}\,\mathrm{N/m}^2$
Poisson's ratio	0.33

Table 2
Geometry and physical properties of the square piezoelectric patches.

Parameter	Value
Dimensions	$50.0 \times 50.0\,\mathrm{mm}^2$
Thickness	0.5 mm
Mass density	$7800\,\mathrm{kg/m}^3$
Young's modulus	$6.25 \times 10^{10}\,\mathrm{N/m}^2$
Poisson's ratio	0.40
Piezoelectric stress constant	$-6.6\,\mathrm{N/V\,m}$

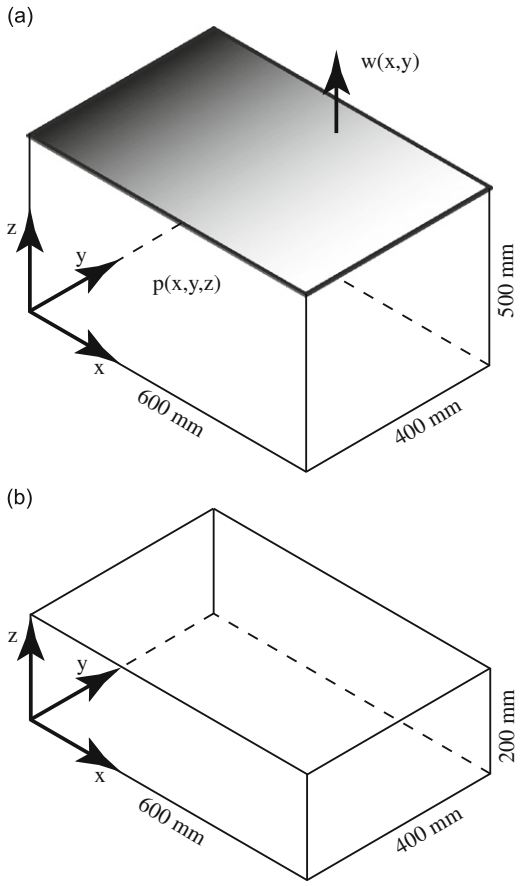

Fig. 1. Sketch of the considered acoustic boxes: (a) cavity 1 and (b) cavity 2. The lateral and bottom walls are rigid.

Table 3
Natural frequencies of the *in vacuo* and fluid loaded plate in the frequency range of interest (400–900 Hz).

in vacuo plate		Rigid-walled cavity		Coupled system	
Mode	Frequency	Mode	Frequency	Mode	Frequency
22	406.11			25	404.20
		4	425.68	26	**427.24**
23	437.99			27	436.17
		5	443.79	28	**445.17**
24	450.69			29	448.93
25	457.73			30	456.19
26	466.04			31	464.58
27	486.49			32	485.28
28	504.57			33	503.11
		6	511.47	34	**512.32**
29	516.98			35	514.98
30	529.37			36	527.78
31	531.57			37	529.61
32	542.60			38	541.17
		7	545.67	39	**547.64**
33	555.30			40	553.43
		8	568.29	41	**569.57**
34	615.52			42	613.86
		9	614.94	43	**616.49**

In bold are highlighted the cavity controlled modes of the coupled system.

wavenumber induced by the acoustic coupling at a certain frequency. In particular, the modal assurance criterion (MAC) is used as a measure of the agreement between the two sets of modes in the 500–700 Hz frequency range. The MAC matrix, illustrated in Fig. 2(a), shows a nearly diagonal behavior indicating that the mode shapes, and hence the associated wavenumbers, of the two systems are virtually the same. Similar conclusions hold for the case in which the same plate is coupled with the smaller enclosure as shown in Fig. 2(b).

As illustrated in Fig. 4 the shapes of panel-controlled natural modes are similar to the *in vacuo* plate modes and the associated cavity mode is slightly perturbed at the interface region to conform with the displacement of the structure. On

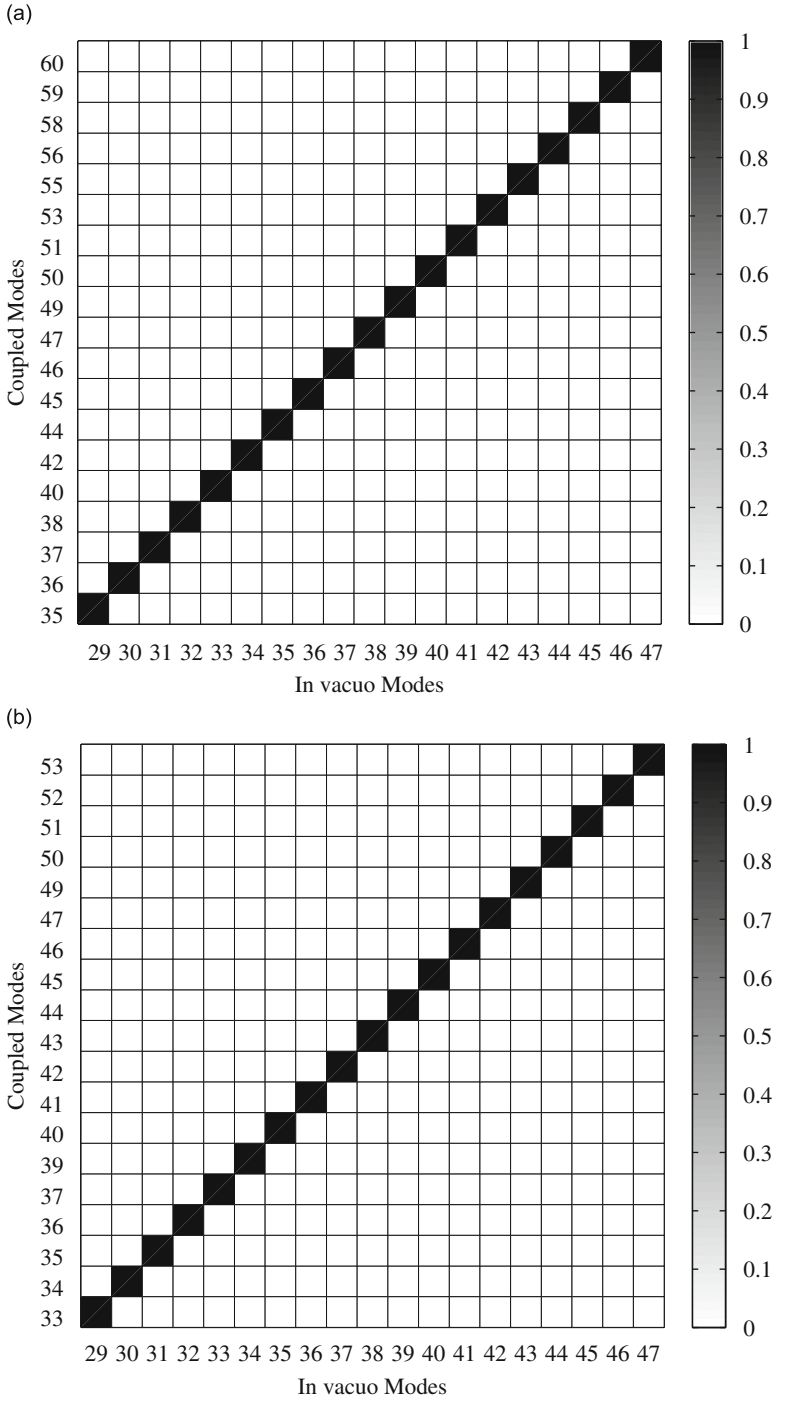

Fig. 2. Modal assurance criterion (MAC) between *in vacuo* and coupled plate controlled modes in the 500–700 Hz range: (a) coupling with cavity 1 and (b) coupling with cavity 2.

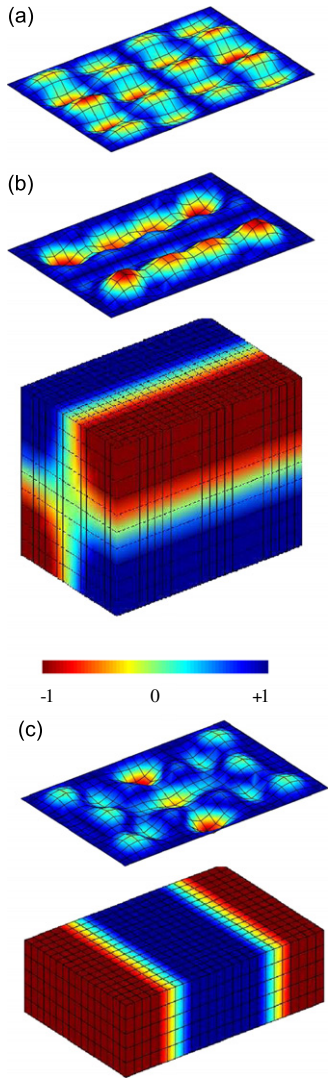

Fig. 3. (a) Deformed shape of the *in vacuo* plate mode 32 (f_n=542 Hz), (b) corresponding cavity-controlled mode when coupled with cavity 1 (f_n=547 Hz), and (c) coupled with cavity 2 (f_n=541 Hz).

the other hand, in the case of cavity-controlled modes, visualized in Fig. 3, the displacement of the structure is significantly distorted to match the pressure distribution of the enclosure.

From these results it can be inferred that only in the case of panel-controlled coupled modes the frequency wavenumber relation of the structure is not significantly altered by the coupling with air cavities, while in the vicinity of cavity-controlled natural frequencies the presence of the enclosure may affect the dispersion properties of the structural waveguide. According to these observations, the dispersion relations of the plate may be computed neglecting, as a first approximation, the loading effect of the fluid into the cavity. The reason for this approximation is two-fold: (1) as shown in Table 3, the modal density of cavity-controlled modes is small relative to structure-controlled modes, and (2) inaccuracies due to this approximation will arise only in the vicinity of cavity-controlled natural frequencies where in any case low control authority can be achieved by means of a mechanical action on the plate [25].

4. Wave propagation in periodic plates

Without the fluid loading effect, wave propagation in 2D periodic structures can be investigated through the analysis of a unit cell (see Fig. 5(b)) and the application of Bloch theorem [26]. This would have been unfeasible if also the complexities introduced by the acoustic coupling in the dynamic stiffness matrix of the system were considered.

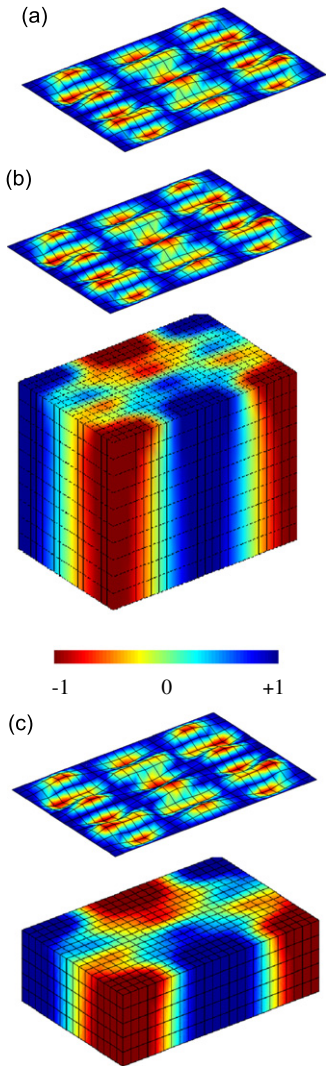

Fig. 4. (a) Deformed shape of the *in vacuo* plate mode 42 (f_n=707 Hz), (b) corresponding panel-controlled mode when coupled with cavity 1 (f_n=704 Hz), and (c) coupled with cavity 2 (f_n=704 Hz).

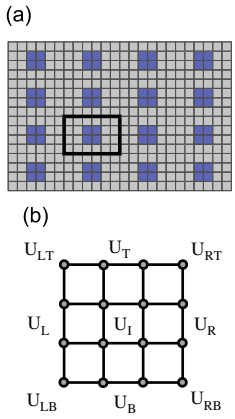

Fig. 5. Schematic of the finite element discretization of a periodic plate (a) and corresponding unit cell (b).

According to what derived in the previous sections, the unit-cell's equation of motion for the piezo-plate without acoustic coupling can be expressed as

$$\mathbf{K}_D(\omega)\mathbf{d} = \mathbf{f} \tag{8}$$

where

$$\mathbf{K}_D(\omega) = \mathbf{K}_{uu} - \omega^2\mathbf{M}_{uu} + \mathbf{S}_{Z_{SH}}(\omega) \tag{9}$$

is the dynamic stiffness matrix and $\mathbf{d}$ and $\mathbf{f}$ are vectors of generalized nodal displacements of the cell and associated forces, respectively. As shown in Fig. 5, the nodal displacements and forces of each cell have been divided according to their relative position in the cell (L—left, R—right, T—top, B—bottom, I—internal). Imposing periodicity conditions on the displacements and equilibrium conditions on the forces yield

$$\mathbf{d} = \mathbf{A}\mathbf{d}^{(r)} \quad \text{and} \quad \mathbf{f} = \mathbf{B}\mathbf{f}^{(r)} \tag{10}$$

where

$$\mathbf{d}^{(r)} = [\mathbf{d}_L \;\; \mathbf{d}_B \;\; \mathbf{d}_{LB} \;\; \mathbf{d}_I]^{\mathrm{T}} \tag{11}$$

$$\mathbf{f}^{(r)} = [\mathbf{f}_L \;\; \mathbf{f}_B \;\; \mathbf{f}_{LB} \;\; \mathbf{f}_I]^{\mathrm{T}} \tag{12}$$

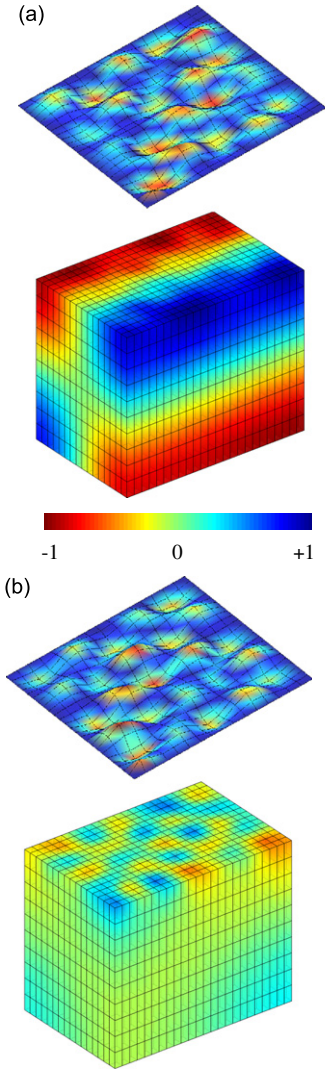

Fig. 6. (a) Operative deformed shape of the coupled panel-cavity system at frequencies close to a cavity-controlled mode (f_n=549 Hz), and (b) a panel-controlled mode (f_n=603 Hz).

are vectors of reduced order. The matrices **A** and **B** are functions of the frequency-dependent propagation constants μ_x and μ_y defined as

$$\mu_k = \delta_k + \mathrm{i}\varepsilon_k \quad (k = x,y) \tag{13}$$

The existence of a real part of the propagation constant indicates that amplitude attenuation occurs as the elastic wave propagates from one cell to the next. For this reason the term δ_k is called *attenuation constant* [26]. Substituting Eqs. (10) into Eq. (8), pre-multiplying the resulting equation by $\mathbf{A}^H$, with H denoting the Hermitian operator, and assuming $\mathbf{f}_I = \mathbf{0}$ yields

$$\mathbf{K}_D^{(r)}(\boldsymbol{\mu},\omega)\mathbf{d}^{(r)} = \mathbf{0} \tag{14}$$

where $\boldsymbol{\mu}$ is the wave vector and $\mathbf{K}_D^{(r)}$ is the reduced dynamic stiffness matrix of the unit-cell. Eq. (14) defines an eigenvalue problem whose solution for assigned $\boldsymbol{\mu}$ yields the corresponding frequency ω of wave propagation:

$$\omega = \omega(\boldsymbol{\mu}) \tag{15}$$

Eq. (14) can be solved by specifying the frequency ω and one of the two wavenumbers and solving for the other, as presented by Spadoni et al. [21].

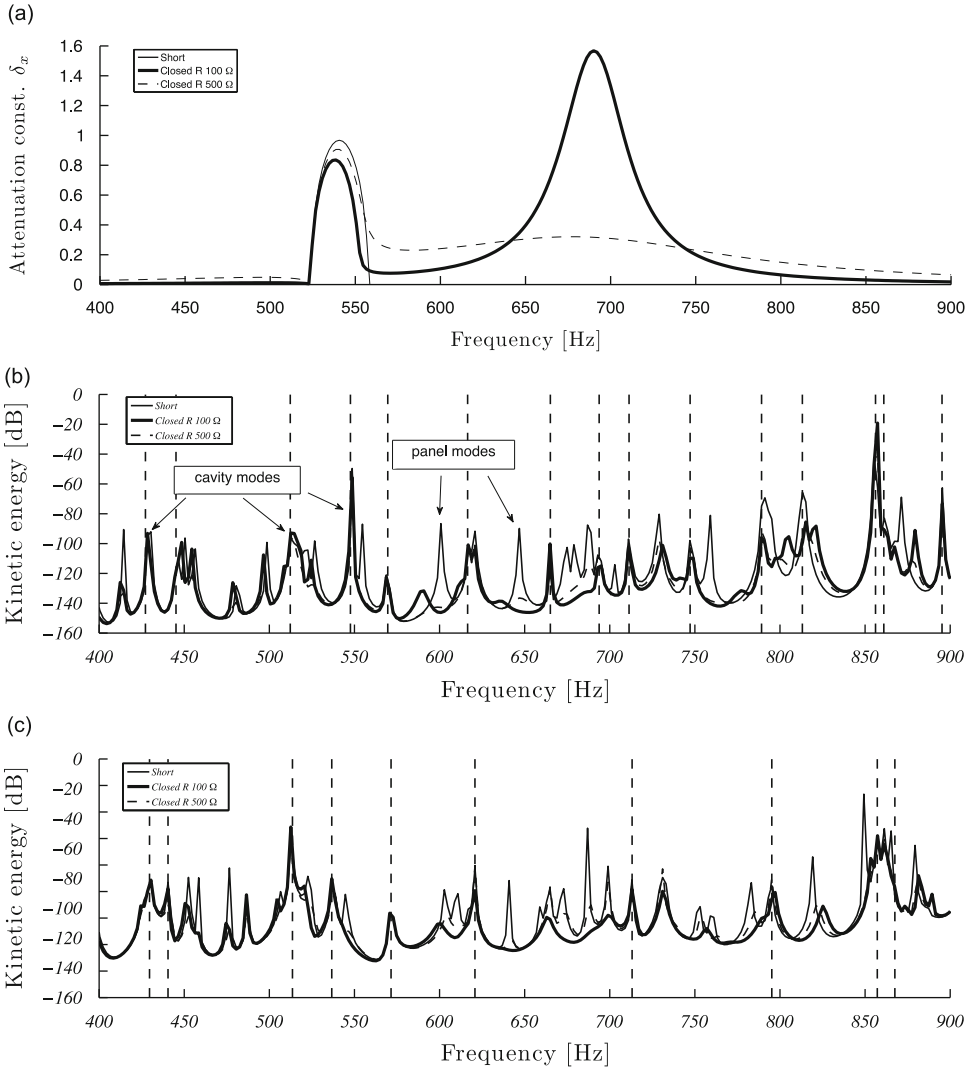

Fig. 7. (a) Attenuation constant δ_x, (b) acoustic kinetic energy inside cavity 1, (c) acoustic kinetic energy inside cavity 2. The RL shunt circuits are tuned at 700 Hz.

5. Numerical analysis of the performance of periodic plate

Numerical results are presented here to assess the method previously outlined. Propagation constants of the periodic piezoelectric plate are evaluated in conjunction with the total kinetic energy of the fluid in the cavity to show the ability of the unit-cell analysis to predict the actual frequency bands of noise reduction. The short circuit configuration, i.e., $Z_{SH} \to 0$, is used as a reference to compare the effects of the shunting circuits.

The host structure consists of a rectangular fully clamped isotropic plate with a periodic array of 4×4 RL-shunted square piezoelectric patches perfectly bonded on one side (see Fig. 5(a)). The geometric and material properties of the plate and piezos are illustrated in Tables 1 and 2. The unit cell features side lengths of 150×100 mm. The flexible structure is forced to vibrate by a point harmonic disturbance located near the lower left corner. Numerical simulations are carried out for the two cavity configurations already considered in Section 3. The total kinetic energy of the fluid, defined as

$$T = \frac{1}{2}\rho_0 \boldsymbol{\phi}^{\mathrm{T}} \mathbf{K}_{pp} \boldsymbol{\phi} \quad \text{where } \partial\boldsymbol{\phi}/\partial t = -\frac{1}{\rho_0}\mathbf{p} \tag{16}$$

is used as a global measure of the sound radiated by the vibrating plate [24]. The FE mesh of the coupled fluid–structure domain includes 384 quadrilateral plate elements and 3840 hexahedral acoustic elements when dealing with the first cavity, and 1920 hexahedral elements for the smaller cavity.

Unit cell analysis is conducted with shunt circuits tuned at $f_{\mathrm{tun}} = 700$ and 1000 Hz, and for two different values of resistances: $R = 100$ and $500\,\Omega$. According to Hagood and Von Flotow [8], for a given frequency f_{tun}, the inductance required

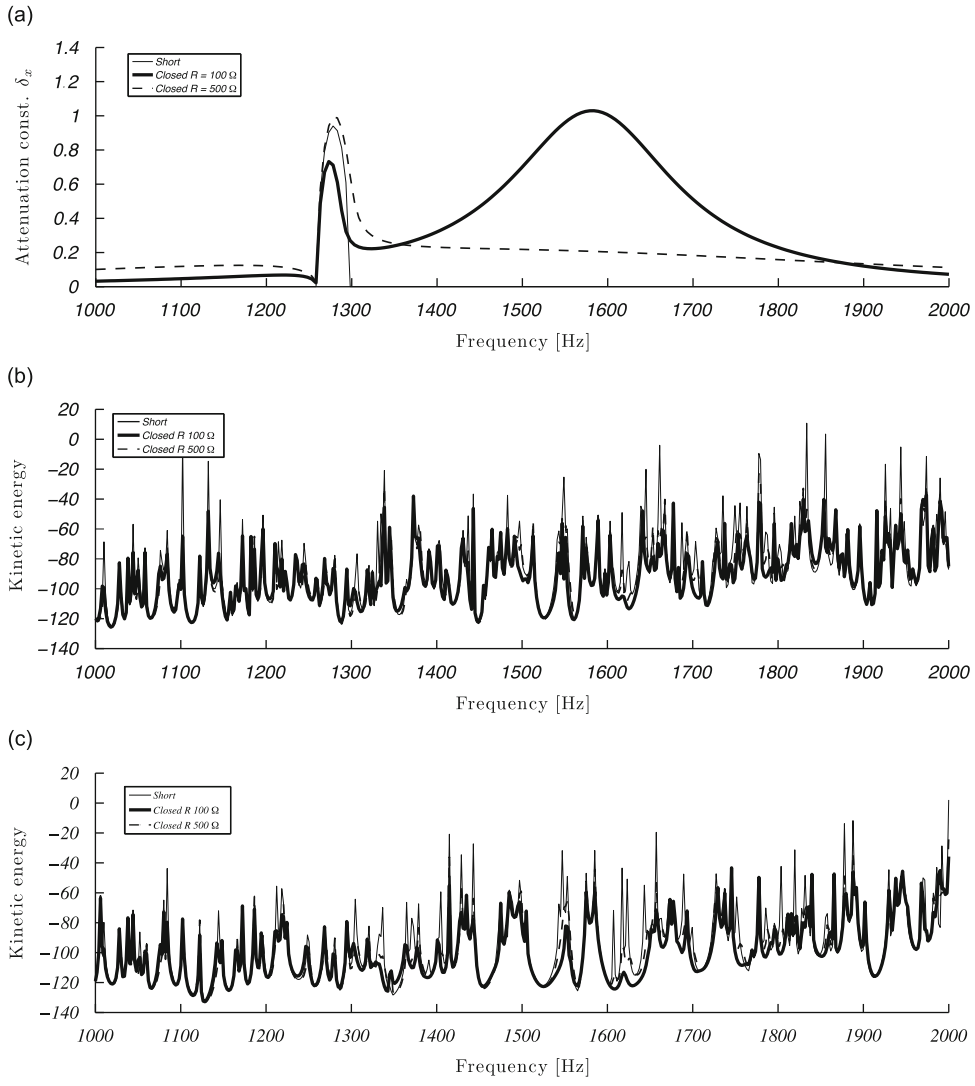

Fig. 8. (a) Attenuation constant δ_x, (b) acoustic kinetic energy inside cavity 1, (c) acoustic kinetic energy inside cavity 2. The RL shunt circuits are tuned at 1600 Hz.

to tune an RL-shunt circuit is given by

$$L = \frac{1}{C_p \omega_{\text{tun}}^2} \tag{17}$$

where C_p is the inherent capacitance of the piezo-patch and $\omega_{\text{tun}} = 2\pi f_{\text{tun}}$ is the tuning frequency. In this work, the selection of the frequencies of attenuation has been driven by the general need to reduce tonal noise components in the bandwidth from 500 to 2000 Hz, which typically characterize the spectrum of structure-borne noise in rotorcraft cabins [27].

Fig. 7(a) shows the variation of the real part of the propagation constant δ_x over the 400–900 Hz range when the shunted circuits are tuned at 700 Hz. As previously stated, attenuation zones are identified by the range of frequencies where the attenuation constant is non-zero. A first attenuation frequency range is shown to be centered around 540 Hz. It remains approximately the same for all circuit configurations and can be attributed to the impedance mismatch generated by the added mass and stiffness of the piezo-patches. In addition, a significant attenuation region can be identified near the shunt tuning frequency covering the range from 550 to 800 Hz. This second range of attenuation is visible only in the closed-circuit configuration and therefore can be associated with the presence of the RL-shunt circuit. The location of this additional attenuation region can be selected by simply varying the inductance of the electrical network without the need to modify the configuration of the structure. Furthermore, it is interesting to observe how the value of the shunted resistance affects the shape of the attenuation bands. From Fig. 7(a) it can be observed that increasing the value of the shunted resistance extends the width of the attenuation region along with a reduction of the maximum attenuation value. This variation can be easily explained by observing that, for the circuit under consideration, the resistance acts as the dissipative term of an equivalent second-order system with resonant frequency regulated by the inductance and capacitance values. The predictions of the unit-cell analysis performed on the periodic structure *in vacuo* are evaluated by computing the harmonic response of the system when the plate is coupled with the enclosure. Fig. 7(b) shows the variation of the total kinetic energy of the fluid in the cavity over the frequency range 400–900 Hz for a tuning at 700 Hz. The short-circuit response is compared with the acoustic response for the two values of shunting resistance. The result confirms that substantial sound radiation reduction is achieved in the frequency ranges predicted by the unit-cell analysis performed on the system *in vacuo*. The location of stop bands in the system frequency response is almost unaffected by the structural-acoustic coupling, which indicates the effectiveness and robustness of the proposed method. According to what observed in the variation of attenuation constants, the amount of noise attenuation depends upon the resistance value of the RL-shunt circuit. Note also that the cavity-controlled modes contained in the attenuation zones are only slightly reduced while the panel-controlled modes are almost completely attenuated. In Figs. 7(b) and (c) the cavity-dominated natural frequencies are highlighted with vertical lines in order to better visualize this idea. Since the present solution is tailored to structural waves, it is effective on panel-controlled modes where most of the energy of the coupled system is stored as structural vibration energy [25].Other control mechanisms should be devised for cavity-dominated modes. Fig. 6 demonstrates the same concept by showing the operative deformed shape of the coupled system when the shunt circuits are tuned at 700 Hz with a resistance of 100 Ω. In particular, Fig. 6 shows that at frequencies close to cavity-controlled

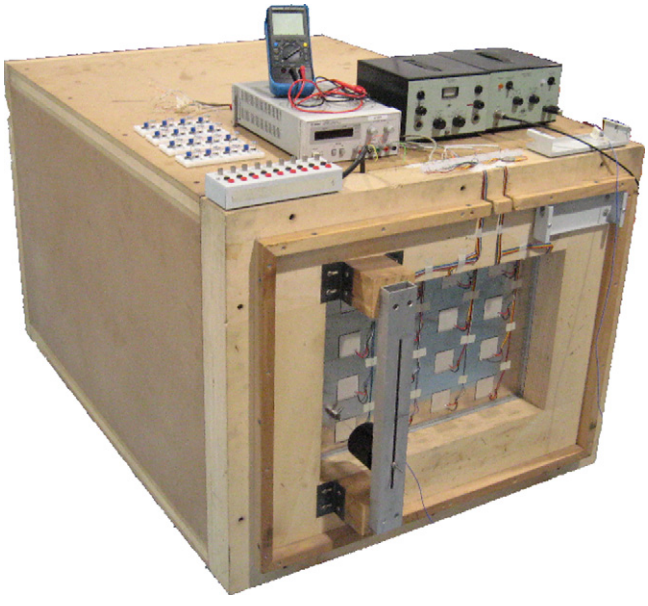

Fig. 9. Photo of the experimental setup.

modes the response is moderately affected by the effect of the shunt circuits while significant attenuation can be achieved in the vicinity of panel-controlled modes.

Similar results are presented in Fig. 8 for a tuning frequency of 1600 Hz. The first attenuation zone in the propagation constant plot is present around 1270 Hz and approximately does not change for all the shunting circuits. This fact confirms that it is to be attributed to the impedance mismatch of the piezos in the short-circuit configuration. A second range of attenuation over the 1300–2000 Hz interval is obtained through piezo-shunts. The predictions based on the *in vacuo* analysis are confirmed by looking at the reduction in the acoustic response of the enclosure. Tuning the RL circuits at higher frequencies introduces a very significant broadband effect since bandwidth increases with the resonant frequency of the considered shunting strategies.

6. Experimental test

This section introduces the design and testing of the periodic smart plate. An aluminum plate with the same geometric properties listed in Table 1 is clamped to a rigid frame fastened to a wooden supporting structure of dimensions 700 $\times$ 500 mm. The resulting assembly is then fixed to a wooden box of depth 1200 mm as illustrated in Fig. 9. The plate is equipped with 16 PZ21 piezoelectric patches (from Ferroperm Piezoceramics) arranged in a regular 4 $\times$ 4 array. Broadband noise in the cavity is generated through a mechanical shaker connected to the flexible plate at point (100,80) mm from the lower left corner. A microphone rack placed in the enclosure facing the plate at a distance of 320 mm maps the related area with a 5 by 4 regular grid.

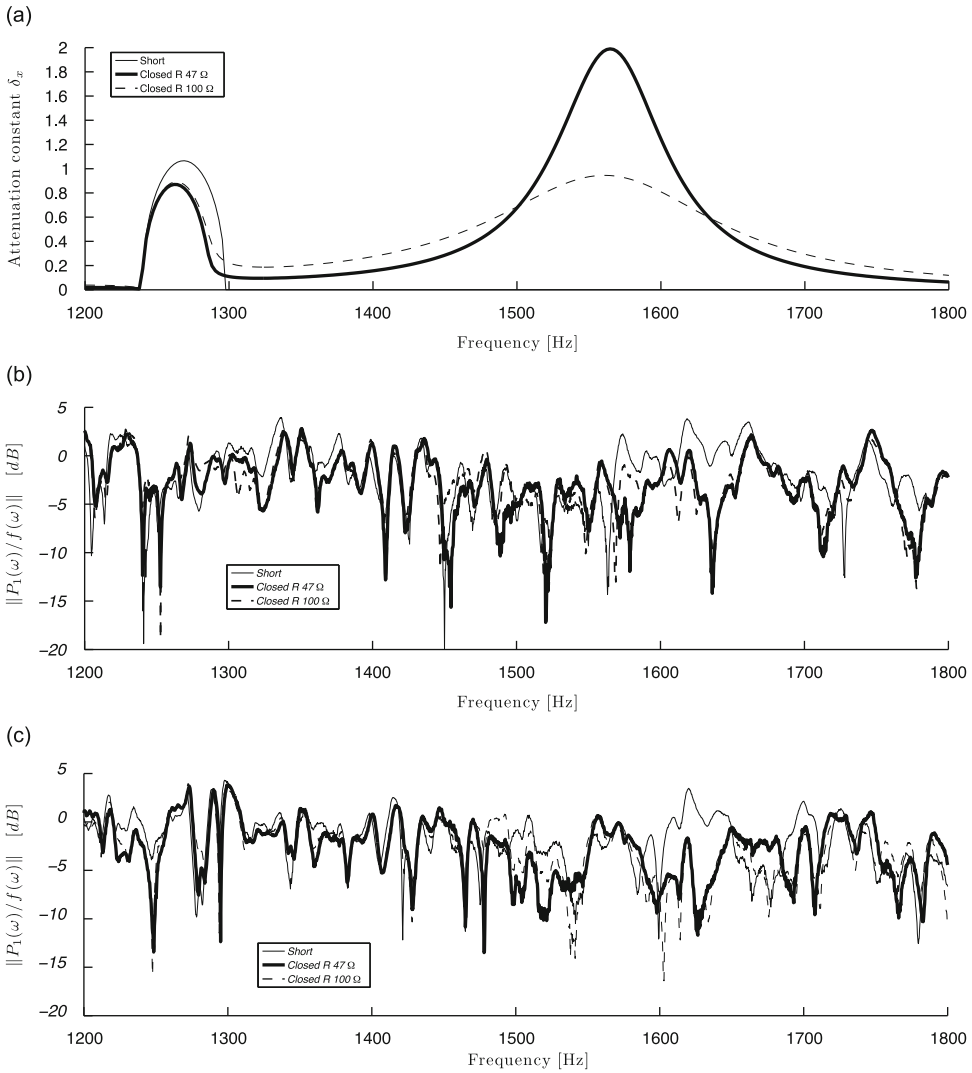

Fig. 10. (a) Attenuation constant δ_x and experimental pressure response functions at locations; (b) 1–(150,150) mm; (c) 2–(520,150) mm.

Results are presented for a tuning frequency of 1600 Hz and two different shunting resistances: $R=47$ and $100\,\Omega$. According to Eq. (17) and the measured value of the piezo-patch capacitance, the required shunting inductance in this case is L=79.464 $\times 10^{-3}$ H. A synthetic inductor as proposed by Antoniou [28] is used in the shunting circuits. The equivalent inductance of the circuit is given by

$$L_{\mathrm{eq}} = \frac{Z_1 Z_3 Z_4 Z_5}{Z_2} \tag{18}$$

where Z_1=R_1, Z_2=R_2, Z_3=R_3, $Z_4 = 1/(\mathrm{j}\omega C)$ and Z_5=R_5 from which it is evident that different inductance values can be easily obtained by simply varying one resistor of the circuit. The components used to obtain the required inductance for the case here considered are the following: $R_1 = 22\,\mathrm{k}\Omega$, $R_2 = 1000\,\mathrm{k}\Omega$, $R_3 = 10\,\mathrm{k}\Omega$, $R_5 = 3612\,\Omega$ and C=100 nF. Fig. 10(a) shows the variation of the attenuation constant δ_x as calculated from the FE unit-cell analysis of the experimental smart plate over the 1200–1800 Hz range. Two attenuation zones are predicted by the model. The first, between 1250 and 1300 Hz, is due to the added mass and stiffness of the piezo. The second zone is generated when the piezos are shunted with RL circuits and is approximately centered around the RL-shunt tuning frequency. Significant attenuation is expected between 1450 and 1700 Hz for lower values of the resistance component.

The numerical predictions of the unit-cell analysis are compared with the pressure response functions measured by the microphones mounted inside the box. Only a small set of measurements are illustrated here as representative of the cavity noise reduction. In particular, Fig. 10 shows the frequency response of two acoustic transducers in response to the excitation introduced by the shaker. Details about sensor locations are reported in the figure caption. The short-circuit responses are compared with the acoustic responses for the two values of shunting resistance. The results are in fairly good agreement with the numerical analysis. Broadband noise reduction is obtained over the attenuation zones predicted by the model. Higher performance are achieved near the RL-shunt tuning frequency and with the lowest value of the resistance, where a maximum 12 dB reduction of the pressure level is achieved. Note that the experimental acoustic response inside the box is relatively well damped even with short-circuited piezos. However, the solution proposed in this work can attain further significant improvements over tunable frequency bands.

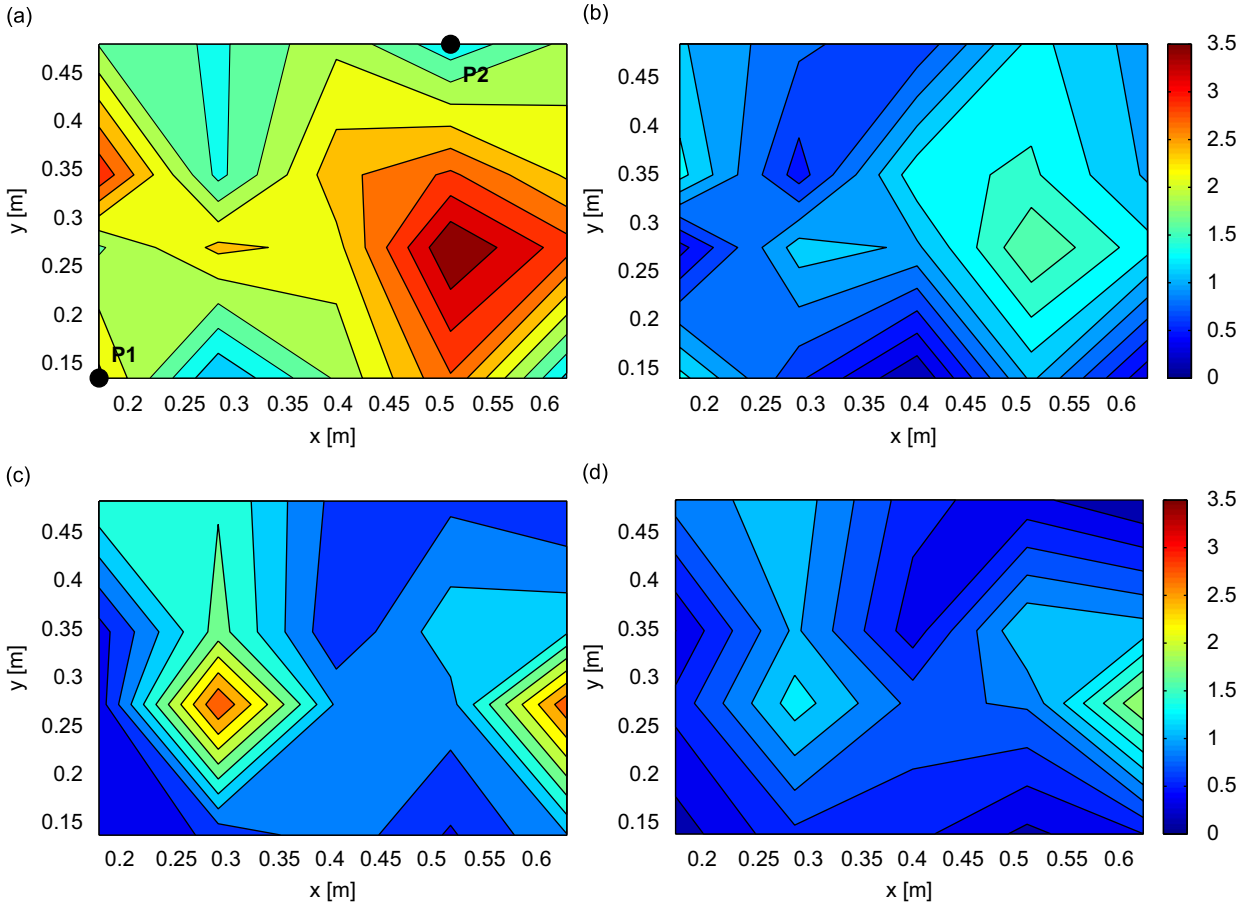

Fig. 11. Spatial pressure distribution at different frequencies. Comparison between the short circuit case (a), (c) and closed circuit case with shunting resistance $R=47\,\Omega$ (b), (d).

Figs. 11(a) and (b) illustrate two maps of the spatial pressure distribution at 1600 Hz obtained with the simultaneous use of all the microphones data. In particular, a comparison between the short and shunted circuits is made in order to appreciate the spatial effect of this control strategy. Similarly, Figs. 11(c) and (d) show the spatial pressure map at 1430 Hz and testifies that noise attenuation may also be achieved far from the tuning frequency.

7. Conclusions

The tuning capabilities of simple RL shunt circuits are combined with filtering characteristics of periodic structures to obtain a tunable periodic plate. The resultant smart structure experiences significant reductions in its noise radiation capability. Numerical simulations demonstrate the applicability of Bloch theorem for unit-cell analysis on the *in vacuo* plate as a tool to predict the frequency ranges of effective structural acoustic control. Finally, experiments are performed to validate the numerical predictions, and to demonstrate the effectiveness of the proposed strategy.

Acknowledgments

This work is supported by a collaborative research agreement (NNX07AD20A) between NASA Langley Research Center and the Georgia Institute of Technology. The authors wish to thank Mr. E. Vigoni from the Politecnico of Milano for his support during the experimental tests.

References

[1] R.J. Bernhard, M. Moeller, S. Young, Automobile, bus, and truck interior noise and vibration prediction and control, in: M.J. Crocker (Ed.), *Handbook of Noise and Vibration Control*, Wiley, New York, 2007.
[2] J.F. Wilby, Aircraft cabin noise and vibration prediction and passive control, in: M.J. Crocker (Ed.), *Handbook of Noise and Vibration Control*, Wiley, New York, 2007.
[3] C.R. Fuller, C.H. Hansen, S.D. Snyder, Active control of sound radiation from a vibrating rectangular panel by sound sources and vibration inputs: an experimental comparison, *Journal of Sound and Vibration* 145 (1991) 195–215.
[4] C.R. Fuller, S.D. Snyder, C.H. Hansen, R.J. Silcox, Active control of interior noise in model aircraft fuselages using piezoceramic actuators, *AIAA Journal* 30 (1992) 2613–2617.
[5] L. Dozio, G.L. Ghiringhelli, Experiments on active vibration and noise reduction of a panel using predictive techniques, *Structural Control and Health Monitoring* 15 (2008) 1–19.
[6] C. Gonzales Diaz, C. Paulitsch, P. Gardonio, Smart panel with active damping units. Implementation of decentralized control, *Journal of the Acoustical Society of America* 124 (2008) 898–910.
[7] N. Quaegebeur, P. Micheau, A. Berry, Decentralized harmonic control of sound radiation and transmission by a plate using a virtual impedance approach, *Journal of the Acoustical Society of America* 125 (2009) 2978–2986.
[8] N.W. Hagood, A. Von Flotow, Damping of structural vibrations with piezoelectric materials and passive electrical network, *Journal of Sound and Vibration* 146 (1991) 243–268.
[9] J.J. Hollkamp, Multimode passive vibration suppression with piezoelectric materials and resonant shunts, *Journal of Intelligent Materials Systems and Structures* 5 (1994) 49–57.
[10] S.Y. Wu, Method for multiple mode shunt damping of structural vibration using a single PZT transducer, *Proceedings of SPIE* 3327 (1998) 159–168.
[11] S. Behrens, A.J. Fleming, S.O.R. Moheimani, A broadband controller for shunt piezoelectric damping of structural vibration, *Smart Materials and Structures* 12 (2003) 18–28.
[12] R.L. Forward, Electronic damping of vibrations in optical structures, *Journal of Applied Optics* 18 (1979) 690–697.
[13] B. de Marneffe, A. Preumont, Vibration damping with negative capacitance shunts: theory and experiment, *Smart Materials and Structures* 17 (2008) 035015.
[14] M. Ahmadian, K.M. Jeric, On the application of shunted piezoceramics for increasing acoustic transmission loss in structures, *Journal of Sound and Vibration* 243 (2001) 347–359.
[15] J. Kim, J.-K. Lee, Broadband transmission noise reduction of smart panels featuring piezoelectric shunt circuits and sound-absorbing material, *Journal of the Acoustical Society of America* 112 (2002) 990–998.
[16] J. Kim, J.-H. Kim, Multimode shunt damping of piezoelectric smart panel for noise reduction, *Journal of the Acoustical Society of America* 116 (2004) 942–948.
[17] J. Kim, Y.-C. Jung, Piezoelectric smart panels for broadband noise reduction, *Journal of Intelligent Materials Systems and Structures* 17 (2006) 685–690.
[18] J. Kim, Y.-C. Jung, Broadband noise reduction of piezoelectric smart panel featuring negative-capacitive-converter shunt circuit, *Journal of the Acoustical Society of America* 120 (2006) 2017–2025.
[19] O. Thorp, M. Ruzzene, A. Baz, Attenuation and localization of wave propagation in rods with periodic shunted piezoelectric patches, *Smart Materials and Structures* 10 (2001) 979–989.
[20] O. Thorp, M. Ruzzene, A. Baz, Attenuation of wave propagation in fluid-loaded shells with periodic shunted piezoelectric rings, *Smart Materials and Structures* 14 (2005) 594–604.
[21] A. Spadoni, M. Ruzzene, K.A. Cunefare, Vibration and wave propagation control of plates with periodic arrays of shunted piezoelectric patches, *Journal of Intelligent Materials Systems and Structures* 20 (2009) 979–990.
[22] F. Casadei, M. Ruzzene, L. Dozio, K.A. Cunefare, Broadband vibration control through periodic arrays of resonant shunts: experimental investigation on plates, *Smart Materials and Structures* 19 (2010).
[23] R.D. Cook, D.S. Malkus, M.E. Plesha, R.J. Witt, *Concepts and Applications of Finite Element Analysis*, fourth ed., Wiley, New York, 2002.
[24] F. Fahy, P. Gardonio, *Sound and Structural Vibration. Radiation, Transmission and Response*, second ed., Elsevier, London, 2007.
[25] J. Pan, D.A. Bies, The effect of fluid–structural coupling on sound waves in an enclosure—theoretical part, *Journal of the Acoustical Society of America* 87 (1990) 691–707.
[26] L. Brillouin, *Wave Propagation in Periodic Structures*, Dover, New York, 1946.
[27] T.A. Millott, W.A. Welsh, C.A. Yoerkie, D.G. MacMartin, M.W. Davis, Flight test of active gear-mesh noise control on the S-76 aircraft, *Proceedings of the 54th AHS Forum*, 1998.
[28] A. Antoniou, Realization of gyrators using operational amplifiers and their use in RC-active-network synthesis, *Proceedings of IEEE* 116 (1969) 1838–1850.